Motion Retargeting for Humanoid Robots Based on Simultaneous Morphing Parameter Identification and Motion Optimization

Ko Ayusawa, *Member, IEEE*, and Eiichi Yoshida, *Senior Member, IEEE*

***Abstract*—This paper presents a novel method for retargeting human motions onto a humanoid robot. The method solves the following three simultaneous problems: the geometric parameter identification that morphs the human model to the robot model, motion planning for a robot, and the inverse kinematics of the human motion-capture data. Simultaneous solutions can imitate the original motion more accurately than conventional approaches, which solve the problems sequentially. The proposed method can reconstruct the human motion within the physical constraints imposed by robot dynamics. A reconstruction step enables quantitative analysis of the retargeting results through direct comparison with the original human motion. The method can also provide the precise morphing function as well as subject-specific models, which can handle the different body dimensions of human subjects. This new framework is suitable for applications that require an accurate generation of human-like motions with quantitative evaluation criteria, such as humanoid robots that evaluate assistive devices. Experimental tests of the proposed method were performed with humanoid robot HRP-4.**

***Index Terms*—Human motion capturing, humanoid robot, identification, motion retargeting, optimization.**

I. Introduction

HUMANOID robots have recently attracted growing social attention because of their technical progress in hardware and software and increasing performance expectations for applications such as disaster response [1] and human interaction [2], [3]. Robots that move like humans are well suited for executing several tasks in environments originally designed for human use. Humanoid motion can also enable a robot to perform entertainment functions like dancing. Recently, humanoid robots have been employed in the evaluation of assistive devices. This application uses a robot's sensing capabilities together with active mobility, unlike crash test dummies [4], [5]. Techniques involved in generating human-like motions for a robot can also be applied to motion generation for digital human models [6], [7], which can in turn be useful in the design of assistive devises [8], [9].

For these applications, robots must mimic human-like motion with as much accuracy as possible. This imitation is complicated by differences in the body structure and mechanical properties between humanoid robots and human bodies. Several recently developed humanoid robots approximate human morphology quite closely [10], [11], and the correspondence of body parts streamlines the imitation of human motion. However, the joint configuration of such robots still differs from that of the human body. Therefore, motions must be translated between different morphologies of humanoid figures while preserving important features. This technique is called motion retargeting. Such a mapping process also requires researchers to quantify the similarity of the generated motion to the original human motion. Without such quantitative feedback, researchers lack clear measures to inform judgments about the best humanoid motion and the optimal process for generating it. Quantitative measures of similarity also encourage fundamental understanding of human motion and allow flexible simulations of motion for different body properties. In some applications such as human-oriented product design or the evaluation of assistive devices, the quantitative analysis of the generated motion is especially important. Quantitative data are necessary, for example, in setting industrial standards for purposes such as product promotion. Therefore, this paper focuses on producing accurate mappings of human-like motions while developing a quantitative comparison framework to evaluate the accuracy of the resulting retargeted motion.

Motion retargeting techniques have been widely investigated for character animations in the field of computer graphics, and for generating robot motion [2], [3], [12]–[20]. In typical applications, human motions are first measured using a motion-capture system, and then the motion data are mapped onto three-dimensional characters or robots. Retargeting techniques combine two main processes, morphing and motion reproduction [12]. The morphing process takes account of the differences in body structure between the human and the retargeted subject, while the motion reproduction process maps the motion with the geometrical and mechanical consistency of the retargeted subject.

When retargeting human motion onto a humanoid robot, there are several considerations: the differences between geometric parameters, range-of-motion limitations in the robot joints, and

Manuscript received June 25, 2017; accepted July 2, 2017. Date of publication October 9, 2017; date of current version December 14, 2017. This paper was recommended for publication by Editor A. Billard upon evaluation of the reviewers' comments. This work was supported in part by METI/AMED Robotic Devices for Nursing Care Project and in part by JSPS Grant-in-Aid for Young Scientists (B) Number 25820082 and JSPS Grant-in-Aid for Scientific Research (A) Number 17H00768. *(Corresponding author: Ko Ayusawa.)*

The authors are with the CNRS-AIST Joint Robotics Laboratory, UMI3218/RL, Tukuba-shi 3058560, Japan (e-mail: k.ayusawa@aist.go.jp; e.yoshida@aist.go.jp).

This paper has supplementary downloadable material available at http://ieeexplore.ieee.org.

Digital Object Identifier 10.1109/TRO.2017.2752711

constraints upon the center of mass (COM) or zero-moment point (ZMP) [21] that maintain stable locomotion. Several approaches have been proposed for retargeting motion from humans to humanoid robots. Ott *et al.* [14] and Miura *et al.* [3] executed the morphing process by attaching virtual markers to a robot model and solving inverse kinematics or static equilibrium equations directly. Nakaoka *et al.* proposed another method that fits the motion-capture data to the robot body in advance using optimization techniques [18], [19]. After the morphing process, motion must be generated in a way that preserves mechanical and dynamic consistency. These two process are usually executed sequentially. Geometric morphing is applied first, followed by adjustments to meet dynamic constraints such as torque limits on robot components or differences in balancing [17], [19]. Several balance controllers have also been proposed for maintaining dynamic stability, because the retargeted motion is often physically inconsistent with the mass distribution of the robot [3], [16]. Several efficient retargeting techniques enable retargeting of walking and dancing motions to humanoid robots [2], [3] and some allow real-time implementation [14], [15], [20].

Previous studies have, in general, focused on producing human-like robot motion from measurements of actual human motion, but most lack a quantitative framework that can analyze the similarity of the generated motion to the original human motions. Without such a framework, there is no guarantee that the retargeted motion is similar in relevant respects to the original human motion. We have previously investigated the evaluation process as a motion-optimization problem, and proposed a novel framework that evaluates how well a retargeting process preserves salient features of the original human motions, such as the trajectories of each joint or body segment [22].

Our retargeting method uses the general retargeting problem reported in [12]. Each constraint condition for robot motion has been introduced in previous related studies. The present study includes four main innovations. First, the identification step estimates both the geometric parameters of each subject and the morphing parameters during the retargeting process, and maintains physical consistency for the robot motion. Each of these problems is dealt simultaneously by solving a single optimization problem. Simultaneous optimization offers better performance in accurately imitating human motions. Second, simultaneous optimization can provide not only the robot motion but also a corresponding virtual human motion; the method reconstructs the retargeted robot motion as if a digital human model were performing the motion. The reconstructed human motion reflects the modifications made for physical consistency during the retargeting process. Our motion-optimization framework enables quantitative analysis of the retargeting results including force information through direct comparisons between the original and reconstructed human motions. We introduced a process for reconstruction of virtual human motion, which we neglected in our previous work [22]. Third, the geometric identification step finds both subject-specific parameters for each human performer and the optimal morphing parameters from each human body to the robot frame. In contrast with conventional heuristic methods, our method is practical because it allows for automatic adjustments. Fourth, a redundant-jointed human model is employed in our morphing process by formulating the mapping function implicitly. In our previous work [22], the morphing process used a one-to-one mapping function for joint angles and orientations. However, such explicit formulas are difficult to handle when the human source and humanoid robot differ in kinematic structure. In this paper, we designed an implicit mapping function based on feature points. Redundant joints in a human, such as shoulders or spines, are constrained after mapping to the robot model and serve as parameters in the mapping function. The optimal angles for such redundant joints, which depend on the outcome of retargeting, can be computed automatically in solving the simultaneous optimization problem. This feature of our process enriches the morphing representation and enhances performance when retargeting motion that involves human joints more complex than their joint analogs. Since our pilot study [22] could not process an implicit formulation of the mapping function, we were unable to investigate this fourth feature of our process sufficiently until now.

The rest of this paper is organized as follows. Section II describes the formulation of our retargeting method with detail discussions of the morphing problem, motion plaining for a robot, and the inverse kinematics of a human model. Section III details the objective function and the constraints used in the optimization problem. The computational implementation is also addressed in Section III. Section IV reports experimental results from tests that retarget captured human motions onto a humanoid robot. Section V presents our conclusions and suggestions for future research.

II. Motion Retargeting to Preserve and Reconstruct Human Motion

This section introduces a general formulation of the retargeting problem as a combination of three subproblems: the morphing problem of mapping a human body to a robot frame, the problem of planning physically consistent motion in the robot, and the inverse kinematics problem for the human model to execute measured movements.

In this paper, let us model both a humanoid robot and a human body as rigid multibody systems. We assume that the following relationship between the two systems holds:

$$\boldsymbol{g}(\boldsymbol{q}_r, \boldsymbol{q}_h, \boldsymbol{\phi}) = \boldsymbol{0} \tag{1}$$

where $\boldsymbol{q}_h$ represents the generalized coordinates of the human system, $\boldsymbol{q}_r$ represents the coordinates of the robot system, and $\boldsymbol{\phi}$ represents the unknown model parameters. Equation (1) indicates how to map (or "morph" [12]) the coordinate system of each body segment from the human and to the robot, and vice versa. In what follows, all model parameters for the robot are assumed to be known because they can be provided by manufacturers.

The unknown parameter set $\boldsymbol{\phi}$ contains the geometric parameters of human body segments in order to accommodate variation between human individuals. Even though they can actually be measured or identified in advance, $\boldsymbol{\phi}$ also includes constant geometric parameters that appears in the mapping function. Let us consider a human model whose geometric parameters can

be changed. This stretchy model can be morphed into the robot model by changing the geometric parameters. In this case, such geometric parameters are also included in the unknown parameter set $\boldsymbol{\phi}$ (they are defined as $\boldsymbol{\phi}_m$ in the next section).

Let $\boldsymbol{q}_{h,t}$ and $\boldsymbol{q}_{r,t}$ be the generalized coordinates of the human and the robot, respectively, at time instances $t = t_1, t_2, \ldots, t_{N_T}$. The trajectories of the two systems are then defined as $\boldsymbol{Q}_h \triangleq [\boldsymbol{q}_{h,1}{}^T \cdots \boldsymbol{q}_{h,N_T}{}^T]^T$ and $\boldsymbol{Q}_r \triangleq [\boldsymbol{q}_{r,1}{}^T \cdots \boldsymbol{q}_{r,N_T}{}^T]^T$. Let us assume the following inequality constraint about trajectories $\boldsymbol{Q}_r$:

$$\boldsymbol{h}(\boldsymbol{Q}_r) \leq \boldsymbol{0}. \tag{2}$$

Equation (2) states the constraints necessary for controlling the robot. For example, the robot needs to operate its joints within mechanical limits and maintain balance with reference to its COM or ZMP. The robot also needs to execute tasks such as reaching to a designed target. In this sense, (2) contains the motion planning problem for the robot. Note that though (2) is formulated as a set of inequality constraints, equality constraints can also be included in (2).

Next, we consider the following optimization problem:

$$\min_{\boldsymbol{Q}_h, \boldsymbol{\phi}} f(\boldsymbol{P}_h, \widehat{\boldsymbol{P}}_h(\boldsymbol{Q}_h, \boldsymbol{\phi})) \tag{3}$$

where $\boldsymbol{P}_h$ represents the given human motion-capture dataset and $\widehat{\boldsymbol{P}}_h$ represents the estimated model of $\boldsymbol{P}_h$ from trajectories $\boldsymbol{Q}_h$ and model parameters $\boldsymbol{\phi}$. Equation (3) indicates the inverse kinematics problem of computing human joint trajectories $\boldsymbol{Q}_h$ while identifying human body segment lengths $\boldsymbol{\phi}$ [23]–[25]. The objective function f can be implemented as, for instance, the mean-square-error normalization between the measured marker positions and those projected by the model. Another example of the cost function is the error function for Laplacian deformation energy [18], [19].

Finally, we formulate the retargeting problem with the following statement of an optimization problem and constraints [22]:

$$\begin{aligned} \min_{\boldsymbol{Q}_h, \boldsymbol{Q}_r, \boldsymbol{\phi}} \quad & f(\boldsymbol{P}_h, \widehat{\boldsymbol{P}}_h(\boldsymbol{Q}_h, \boldsymbol{\phi})) \\ \text{subject to} \quad & \widehat{\boldsymbol{g}}(\boldsymbol{Q}_h, \boldsymbol{Q}_r, \boldsymbol{\phi}) = \boldsymbol{0} \\ & \boldsymbol{h}(\boldsymbol{Q}_r) \leq 0 \end{aligned} \tag{4}$$

where $\widehat{\boldsymbol{g}}$ concatenates (1) for all times.

Let us clarify the benefit that the formulation in (4) affords in mimicking human motion as closely as possible. As reviewed above, several retargeting methods separate the mapping and the motion planning processes [3], [13], [18], [19], which is almost equivalent to solving the following problems sequentially:

$$\begin{aligned} \min_{\boldsymbol{Q}_h, \widehat{\boldsymbol{Q}}_r, \boldsymbol{\phi}} \quad & f(\boldsymbol{P}_h, \widehat{\boldsymbol{P}}_h(\boldsymbol{Q}_h, \boldsymbol{\phi})) \\ \text{subject to} \quad & \widehat{\boldsymbol{g}}(\boldsymbol{Q}_h, \widehat{\boldsymbol{Q}}_r, \boldsymbol{\phi}) = \boldsymbol{0} \end{aligned} \tag{5}$$

$$\begin{aligned} \min_{\boldsymbol{Q}_r} \quad & \widehat{f}(\widehat{\boldsymbol{Q}}_r, \boldsymbol{Q}_r) \\ \text{subject to} \quad & \boldsymbol{h}(\boldsymbol{Q}_r) \leq 0 \end{aligned} \tag{6}$$

where $\widehat{\boldsymbol{Q}}_r$ is an intermediate variable to connect the two problems and function $\widehat{f}$ evaluates the error between $\widehat{\boldsymbol{Q}}_r$ and $\boldsymbol{Q}_r$. The robot trajectory $\widehat{\boldsymbol{Q}}_r$ is obtained by solving (5) first, and can be regarded as a trajectory morphed from the measured human motion. Then, the final trajectory $\widehat{\boldsymbol{Q}}_r$ is computed via the second optimization problem [see (6)]. Usually, the cost function in (6) contains terms that evaluate the difference between the morphed trajectory $\widehat{\boldsymbol{Q}}_r$ and the final trajectory $\widehat{\boldsymbol{Q}}_r$. Let us assume an inverse mapping from $\boldsymbol{Q}_r$ to $\boldsymbol{Q}_h$ under (1). In such a case, the trajectory $\widehat{\boldsymbol{Q}}_r$ of the robot can be converted back to the corresponding trajectory $\widehat{\boldsymbol{Q}}_h$ of the human. However, the converted trajectory $\widehat{\boldsymbol{Q}}_h$ is not guaranteed to be an optimal solution to the original cost function in (3). Solving (4) with both constraints simultaneously can provide a trajectory that is optimized for both close magging and physically consistent robot motion, which leads better performance of motion retargeting.

The second benefit of our method is that it can reconstruct retargeted robot motion as if a human model was performing the motion. The problem shown in (4) can also provide solution for the human trajectory $\boldsymbol{Q}_h$ as well as that for $\boldsymbol{Q}_r$. Let us express the solutions of (4) as $\boldsymbol{Q}_h^*$, $\boldsymbol{Q}_r^*$, and $\boldsymbol{\phi}^*$. The trajectory $\boldsymbol{Q}_h^*$ is different from the solution of the standard inverse kinematics problem for human motion in (3) because $\boldsymbol{Q}_h^*$ has been modified according to the constraints in (1) and (2). The human motion dataset can also be reconstructed by computing

$$\boldsymbol{P}_h^* = \widehat{\boldsymbol{P}}_h(\boldsymbol{Q}_h^*, \boldsymbol{\phi}^*) \tag{7}$$

where $\boldsymbol{P}_h^*$ represents the reconstructed dataset. Let us assume that we can obtain human motion data that satisfy $\boldsymbol{P}_h = \boldsymbol{P}_h^*$ under ideal conditions. When $\boldsymbol{Q}_h = \boldsymbol{Q}_h^*$ and $\boldsymbol{\phi} = \boldsymbol{\phi}^*$ hold, the error between $\boldsymbol{P}_h$ and $\widehat{\boldsymbol{P}}_h$ is equal to zero and the cost function in (3) is effectively minimized. If $\boldsymbol{P}_r = \boldsymbol{P}_r^*$ also holds, all constraints in (4) will be satisfied. This exercise shows that, when we are able to capture datasets such as $\boldsymbol{P}_h = \boldsymbol{P}_h^*$, the solutions of (3) and (4) are expected to be the same without redundancy problems. Therefore, the reconstructed dataset $\boldsymbol{P}_h^*$ reflects the modifications that are made during the retargeting process. By comparing the reconstructed human motion with the originally captured human motion, our method provides a framework for evaluating the imitation effectiveness of the retargeted motion by comparing apples to apples, as it were.

The proposed framework does not conflict with other approaches; with (2), we can still follow previous studies and combine the constraints with strong optimization techniques for motion generation [17], [19]. The proposed method can extend this process to the simultaneous optimization problem by introducing an implicit formulation of the morphing function in (1) when identifying geometric parameters.

In the proposed framework, the mapping function is written in an arbitrary implicit form with respect to the joint coordinates and morphing parameters. Therefore, a human model can have a different number of degrees of freedom (DOFs) that does the target robot. The human model can have redundant joints not found in humanoid robots, such as sternoclavicular joints or spines. Let $\boldsymbol{q}_h^r$ represent such redundant joint angles. They are constrained to certain values $\boldsymbol{q}_h^{r*}$ during the morphing

process. Though $\boldsymbol{q}_h^{r*}$ is not included in $\boldsymbol{\phi}$, it can also serve as a set of pseudomorphing parameters that enrich the representation archived by the morphing function. Note also that the values of $\boldsymbol{q}_h^{r*}$ depend on the particular kind of motion that is being retargeted, and are difficult to determine in advance. For example, the human shoulder consists of several joints. If the shoulder is approximated as one spherical joint, the position of its joint center should vary according to the actual posture of the redundant shoulder joints. Our framework provides optimal values for $\boldsymbol{q}_h^{r*}$ in terms of (4), which can improve the results when retargeting the movement of shoulders and other complex human articulations.

Note that the proposed framework does not evaluate whether (4) itself captures the best similarity metric for postures or motions in the same sense as that of human perceived judgments of similarity, as mentioned in [26]. When the similarity metric is assumed to be included in the cost function in (4), our method can provide the optimal solution according to that metric. The framework enables a quantitative comparative analysis of the retargeting results by checking the modification of the several physical quantities germane to the human model. Each application for the method will take different quantitative measures as relevant.

The main steps in the proposed method are summarized as follows.

1) The method solves three simultaneous problems: the inverse kinematics problem of a human model, the geometric mapping between the human model and a robot, and motion planning for the robot. Our simultaneous optimization algorithm should yield better results than sequential optimization, as it accounts for modifications throughout the retargeting process.
2) Since the identification of geometric parameters is specific to each human subject performing a motion, the method can accommodate the varying body dimensions of individual humans.
3) The method can reconstruct the retargeted motion to produce the virtual human motion that reflects the modifications made during the retargeting process. This reconstruction enables direct comparisons with the original human motion.
4) When using a human model with redundant joints, the angles representing the redundant joints also contribute to the precision of the morphing between the human and robot structures. The proposed method can also provide their optimal values.

A conceptual diagram of this method is presented in Fig. 1. Actual implementations of the cost function and constraints in our optimization problem [see (4)] are detailed in the next section.

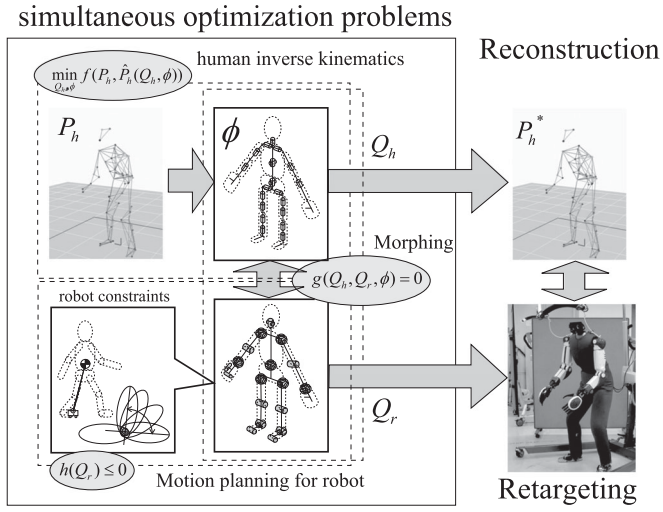

Fig. 1. Conceptual diagram of the proposed motion retargeting method.

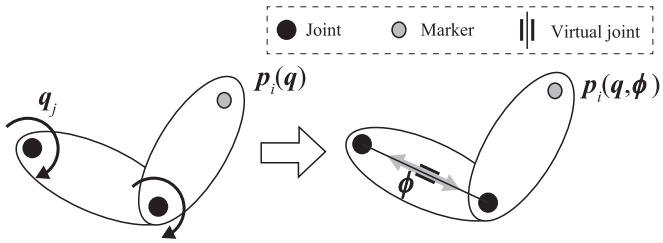

Fig. 2. Virtual joints that represent the geometric parameters of the link structure.

III. Implementation of Optimization Problem

A. Morphing Function

Let us represent the geometric parameters with virtual mechanical joints [25]. Fig. 2 shows an example of representing the distance of the joints with a translational joint connecting them. The benefit of this representation is that $\boldsymbol{\phi}$ can be expressed in the generalized coordinates of the virtual mechanical joints, and we can use the same methods for kinematics computations that we used for mechanical joints.

Let us consider a human model that consists of generalized coordinates $\boldsymbol{q}_h$ and geometric parameters $\boldsymbol{\phi}_h$. To construct a subject-specific human model, $\boldsymbol{\phi}_h$ will be fully specified. We may also introduce another human model by changing only the geometric parameters, as any two human models have the same generalized coordinates but different geometric parameters. Let us refer to the latter model as the morphed model and define $\boldsymbol{\phi}_m$ as its geometric parameters. We now consider the feature points attached on the morphed human model. Let the position of feature point k be represented by the forward kinematics function $\boldsymbol{r}_k(\boldsymbol{q}_h, \boldsymbol{\phi}_h)$.

We also consider a robot model with generalized coordinates $\boldsymbol{q}_r$. We can assume that all geometric and inertial parameters of the robot are given. Let $\boldsymbol{q}_h$ and $\boldsymbol{q}_r$ be represented as

$$\boldsymbol{q}_h = \begin{bmatrix} \boldsymbol{p}_h{}^T & \boldsymbol{\xi}_h{}^T & \boldsymbol{\theta}_h{}^T \end{bmatrix}^T \tag{8}$$

$$\boldsymbol{q}_r = \begin{bmatrix} \boldsymbol{p}_r{}^T & \boldsymbol{\xi}_r{}^T & \boldsymbol{\theta}_r{}^T \end{bmatrix}^T \tag{9}$$

where $\boldsymbol{p}_h$ and $\boldsymbol{p}_r$ are the position vectors of the base-link of the human and robot, respectively, $\boldsymbol{\xi}_h$ and $\boldsymbol{\xi}_r$ represent the quaternion of the orientation of the base-link, and $\boldsymbol{\theta}_h$ and $\boldsymbol{\theta}_r$ be the vectors of the joint angles.

The robot model has feature points that corresponds to the points attached to the morphed model. Let the position of feature point k on the robot be $\boldsymbol{s}_k(\boldsymbol{q}_r)$. In the morphing process, let us maintain the following relationship for all feature points on the robot model and the morphed model:

$$\boldsymbol{s}_k(\boldsymbol{q}_r) = \boldsymbol{r}_k(\boldsymbol{q}_h, \boldsymbol{\phi}_m). \tag{10}$$

By choosing appropriate constant parameters $\boldsymbol{\phi}_m$, the locations of the feature points attached on the morphed model can match those on the robot model. We assume that all joint coordinates of the robot have equivalent coordinates in the human model. In other words, by simplifying the joint coordinates of the morphed model with the appropriate parameters $\boldsymbol{\phi}_m$, the morphed model can realize the same kinematic structure as that of the robot model. Since we have made this assumption as long as $\boldsymbol{q}_r$ is given, we can find at least one solution of $\boldsymbol{q}_h$ that satisfies (10).

During the morphing process, $\boldsymbol{\phi}_h$ and $\boldsymbol{\phi}_m$ are the unknown geometric parameters. Let us concatenate them as vector $\boldsymbol{\phi}$ in the following discussion:

$$\boldsymbol{\phi} = \begin{bmatrix} \boldsymbol{\phi}_h{}^T & \boldsymbol{\phi}_m{}^T \end{bmatrix}^T. \tag{11}$$

The mapping functions are often formulated as one-to-one correspondences between the joint angles or rotations, $\boldsymbol{q}_h$ and $\boldsymbol{q}_r$, as in our previous work [22]. Though such mapping functions allow easy computation, they are less useful for capturing difference in the kinematic structure. Below, we use a formulation based on (10) for retargeting motion from redundant-jointed human model.

B. Evaluation Function for Human Inverse Kinematics

Let $\boldsymbol{p}_{i,t}{}^{\mathrm{ref}}$ $(1 \le i \le N_M,\ 1 \le t \le N_T)$ be the measured position of the ith captured marker at instances $t_1, t_2, \ldots, t_{N_T}$, where N_M is the total number of markers. The captured human motion data $\boldsymbol{P}_h$ consist of $\boldsymbol{p}_{i,t}{}^{\mathrm{ref}}$ for all markers and time instances. We now define the following evaluation function with respect to $\boldsymbol{q}_{h,t}$ $(1 \le t \le N_T)$:

$$f(\boldsymbol{Q}_h, \boldsymbol{\phi}) \triangleq \frac{1}{2} \sum_{t=1}^{N_T} \sum_{i=1}^{N_M} ||\boldsymbol{p}_i(\boldsymbol{q}_{h,t}) - \boldsymbol{p}_{i,t}{}^{\mathrm{ref}}||^2 \tag{12}$$

where $\boldsymbol{p}_i$ indicates the position of the ith marker attached to the human model and $\boldsymbol{p}_i$ is a function of $\boldsymbol{q}_h$ obtained by forward kinematics computation. Equation (12) represents the problem of computing the inverse kinematics of the human joint trajectories and identifying human segment lengths from motion-capture data [25].

Function $\widehat{\boldsymbol{P}}_h$ in the previous section corresponds to the forward kinematics functions $\boldsymbol{p}_i$ and computes the position of the markers attached on the model at all-time instances. Equation (7) is also implemented by computing the forward kinematics functions $\boldsymbol{p}_i$ using the optimized solutions.

C. Physically Consistent Conditions of the Robot

Let us consider the following conditions that limit the joint angles and their derivatives:

$$\boldsymbol{\theta}_{r,\min} \le \boldsymbol{\theta}_r \le \boldsymbol{\theta}_{r,\max} \tag{13}$$

$$\dot{\boldsymbol{\theta}}_{r,\min} \le \dot{\boldsymbol{\theta}}_r \le \dot{\boldsymbol{\theta}}_{r,\max} \tag{14}$$

$$\ddot{\boldsymbol{\theta}}_{r,\min} \le \ddot{\boldsymbol{\theta}}_r \le \ddot{\boldsymbol{\theta}}_{r,\max}. \tag{15}$$

Equation (15) originates from conditions constraining of the joint torques. The dynamics of the motors are often dominant in joints with gears that have a high reduction ratio. In this case, by estimating the maximum load inertia of each joint individually, the upper and lower limits of joint acceleration can be estimated.

Before considering the constraints on the dynamics of the robot, we assume the following about the human motion data and the feet of the robot.

1) All contact states in human motion data are known for all time instances.
2) All motions are always balanced and in contact with the ground.
3) The sole of the robot foot is flat, and the XY plane of the coordinate system of the foot link plane is parallel to the sole.

When the human foot contacts the ground, we add the following condition for the corresponding robot foot:

$$\boldsymbol{R}_{r,\mathrm{foot}} \boldsymbol{e}_z = \boldsymbol{e}_z \tag{16}$$

$$\dot{\boldsymbol{p}}_{r,\mathrm{foot}} = \boldsymbol{0} \tag{17}$$

where $\boldsymbol{p}_{r,\mathrm{foot}} \in \mathbb{R}^3$ $(\mathrm{foot} = r\mathrm{foot}, l\mathrm{foot})$ is the position of the coordinate system attached to the left or right foot, $\boldsymbol{R}_{r,\mathrm{foot}} \in \mathbb{R}^{3\times 3}$ is the orientation matrix, and $\boldsymbol{e}_z = [0\ 0\ 1]^T$.

When both feet contact the ground, the following condition is imposed at the corresponding times:

$$\boldsymbol{e}_z{}^T (\boldsymbol{p}_{r,l\mathrm{foot}} - \boldsymbol{p}_{r,r\mathrm{foot}}) = 0. \tag{18}$$

In this paper, we approximate a ZMP equation for the whole system with a model of a linear inverted-pendulum whose mass is concentrated at the COM and manipulated by ZMP [27], [28]. This equation can be described by

$$\ddot{\boldsymbol{p}}_c = \frac{g}{p_{c,z}} (\boldsymbol{p}_c - \boldsymbol{p}_{\mathrm{zmp}}^{\mathrm{ref}}) \tag{19}$$

where $\boldsymbol{p}_c \in \mathbb{R}^3$ is the position of the COM, $p_{c,z}$ is its z-axis component, g is the constant for acceleration due to gravity, and $\boldsymbol{p}_{\mathrm{zmp}}^{\mathrm{ref}}$ is the desired ZMP of the robot, which is determined from the human motion capture data. $\boldsymbol{p}_{\mathrm{zmp}}^{\mathrm{ref}}$ must satisfy the following constraint:

$$\boldsymbol{p}_{\mathrm{zmp}}^{\mathrm{ref}} \subset \mathbb{P}_{\mathrm{zmp}} \tag{20}$$

where $\mathbb{P}_{\mathrm{zmp}}$ represents the allowable area for the ZMP inside the supporting polygons of the robot feet. The center of pressure (CoP) of the human can be measured or estimated from the motion-capture data. As the human is balanced in contact with ground, CoP can be used directly as a candidate for $\boldsymbol{p}_{\mathrm{zmp}}^{\mathrm{ref}}$. We need to check whether $\boldsymbol{p}_{\mathrm{zmp}}^{\mathrm{ref}}$ satisfies (20). When $\boldsymbol{p}_{\mathrm{zmp}}^{\mathrm{ref}}$ lies outside of the supporting polygons of the robot feet, it is moved

to the nearest point inside the polygon. Though morphing of ZMP will be required when the robot feet are of a totally different shape from that of the human, we assume that the difference is small and can be neglected.

We also assume the following limitation on the center of total mass, in order to maintain static equilibrium in complicated postures when the reference ZMP is unreliable

$$\boldsymbol{p}_c \subset \mathbb{P}_c \tag{21}$$

where $\mathbb{P}_c$ represents the motion range area of the center of total mass, and the supporting area is designed to match this area projected onto the *XY* plane.

The above constraints are mainly focused on the physical consistency and the control issues [22]. However, the robot sometimes needs to achieve particular tasks with its retargeted motion. In a reaching motion, for example, the hand of the robot needs to actually reach the target. Because of the different body properties of a human and a robot, even if the retargeted motion is similar in the joint-angle space, the robot feature point may not reach the target position in Cartesian space. We also consider constraints on the positions of some links such as hands. From a practical viewpoint, we select the subset of markers attached on those links in human motion-capture data. We also select the virtual markers corresponding to the human marker set on the robot model. We now add constraints on the positions of these particular markers as

$$\forall\, j \in \mathbb{S}_m \;\; \boldsymbol{p}_j^{\text{robot}}(\boldsymbol{q}_{r,t}) = \boldsymbol{p}_{j,t}{}^{\text{ref}} \tag{22}$$

where $\boldsymbol{p}_j^{\text{robot}}$ represents the position of the *j*th virtual marker attached on the robot model and $\boldsymbol{p}_j^{\text{robot}}$ is a function of $\boldsymbol{q}_{h,t}$ obtained by forward kinematics computation. $\mathbb{S}_m$ is the set of indices of the selected markers.

D. Implementation of Optimization

Direct optimization of $\boldsymbol{Q}_h$, $\boldsymbol{Q}_r$, and $\boldsymbol{\phi}$ of (4) would entail a huge computation cost because of the large number of variables. The problem would grow more complex than the geometric identification problem [25]. In the standard problem, since the velocities and accelerations need not be considered, we usually select the minimal set of samples of $\boldsymbol{Q}_h$ that allow the identification. In this paper, (4) is solved with the following three implementation choices.

A) The velocities and accelerations are computed by the finite-difference method.
B) All equality and inequality constraints are solved by the penalty-function method [29].
C) The geometric parameters are assumed to be quasi-non-variant.

The derivative of the generalized coordinates at time t can be computed according to (A) as

$$\dot{\boldsymbol{x}}_t = \frac{1}{\Delta t}(\boldsymbol{x}_t - \boldsymbol{x}_{t-1}) \tag{23}$$

$$\omega_t = \boldsymbol{K}(\boldsymbol{\xi}_t)\frac{1}{\Delta t}(\dot{\boldsymbol{\xi}}_t - \dot{\boldsymbol{\xi}}_{t-1}) \tag{24}$$

where $\boldsymbol{x}$ represents the variables except rotation variables and $\boldsymbol{K}(\boldsymbol{\xi}_t)$ is the matrix that converts the derivative of quaternions to angular velocities. The initial velocities and accelerations are considered to be zero.

Let us estimate the initial values for the quasi-non-variant geometric parameters before retargeting. In this paper, we choose several samples from the dataset measured by a motion-capture system, and the initial parameters are computed by solving (12) under (10) and only the constraints on joint angles within the gemetric identification step [25]. Note that the conditions on physical consistency including velocities and accelerations of the robot are ignored in this initial guess. Let the identified values be defined as $\widehat{\boldsymbol{\phi}}$. Strictly speaking, since many human joints are not actually rotational or spherical joints, each length between the joints can change slightly. Therefore, the geometric parameters are assumed to be time-variant according to step (C), and a penalty against $\boldsymbol{\phi}_t$ is added. Finally, (4) can be computed by solving the following problem for all times:

$$\begin{aligned}\min_{\boldsymbol{q}_{h,t},\boldsymbol{q}_{r,t},\boldsymbol{\phi}_t} \; & \frac{1}{2}\sum_{i=1}^{N_M} ||\boldsymbol{p}_i(\boldsymbol{q}_{h,t},\boldsymbol{\phi}_t) - \boldsymbol{p}_{i,t}{}^{\text{ref}}||^2 \\ & + \omega_\phi ||\boldsymbol{\phi}_t - \widehat{\boldsymbol{\phi}}||^2 + \omega_{g_k}\sum_k ||\boldsymbol{s}_k - \boldsymbol{r}_k||^2 \\ & + \omega_{h_l}\sum_l ||\min(0, h_k)||^2 \end{aligned} \tag{25}$$

where h_k represents the individual inequality constraints from (13) to (22), and ω_ϕ, ω_{g_k}, and ω_{h_l} are weighting factors for each penalty term. Each penalty weight is determined according to an allowable violation of the inequality constraint.

Since problem (25) can be regarded as an inverse kinematics problem of two multibody systems, it can be solved by the usual inverse kinematics techniques. The number of variables in (25) is double that required for the normal inverse kinematics problem for one robot. Typical inverse kinematics methods require large computational resources to compute the Jacobian matrix and its inverse. We solve this problem with a fast inverse kinematics method for large-scale multibody systems [30]. The method [30] solves the inverse kinematics problem without computing the Jacobian matrix of each link and its inverse. Instead, this method computes the gradient vector of the cost function by solving the static equilibrium problem and updates the solution through a super-linear method such as a conjugate-gradient method [29]. The computational complexity of each iterative computation in this algorithm is $O(N)$, where N is the number of variables of the problem.

Note that all equality and inequality constraints can be solved for using other methods such as sequential quadratic programming (SQP) [29]. Though the penalty function method allows for violation of the constraints, SQP can obtain a precise solution. We begin to use the penalty function method because our original goal is fast implementation for future applications, such as online retargeting. The retargeting framework contains not only variables for the robot but also those for the human and the geometric parameters; the total DOFs can exceed 100. Since the computational complexity of even the quasi-Newton-SQP is

Fig. 3. Overview of humanoid robot HRP-4 (left). The robot can wear a human assistive device (right).

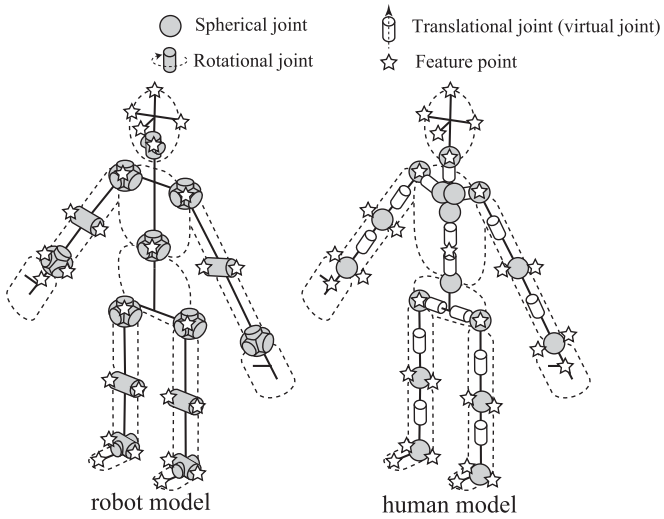

Fig. 4. Joint placements of HRP-4 (left) and a human model (right). The geometric parameters are represented by virtual translational joints (right). The feature points used in the morphing function are shown as star markers (left and right).

much higher, we adopt the above method [30]. Violations of the constraints can also be reduced by increasing the weight of the penalty, and can be neglected with respect to the tracking error of the controllers when the robot actually plays back the motion. However, if accuracy rather than speed is important, when conditions are so severe that the range of the solution is narrow, for example, the proposed framework should be implemented with SQP instead.

IV. Experiments on Retargeting Motion

This section presents the experimental results for the proposed retargeting method. First, we report the results of several retargeted motions that can be performed by an actual robot. Then, the advantage of the simultaneous optimization of (4) is demonstrated with an example situation in which our method offers better performance than the results of solving (5) and (6) sequentially. To validate our method's effectiveness, the reconstructed human motions are compared to the original motion-capture data. The performance of our framework is assessed with an example of retargeting arm movements performed by a model with redundant shoulder joints. We finally demonstrate that the geometric parameter identification accommodates retargeting from several different sizes of human subjects.

A. Experimental Setup

The proposed method was tested with humanoid robot HRP-4 [11]. An overview of the robot is shown on the left side of Fig. 3. Though the original body surface of HRP-4 is made of hard plastic covers, we replaced the covers with a soft suit in order to mimic a human body surface. The geometric properties of HRP-4 are also designed to be close to the measured average of humans. This similarity enables the robot to wear clothes or devices designed for humans. The right side of Fig. 3 shows the robot wearing an assistive device [8] for evaluating the device. Though the total DOF of the robot is originally 34 [11], our robot has a roll joint at the waist. The finger joints were fixed for the whole retargeting process; therefore, the total robot DOF for our experiments was 31. The placements of the joints that we use are illustrated on the left side of Fig. 4.

We also used the human skeletal model as reported in [6], [22]. Though the original DOF of the model exceeds 100, some joints of the model can be fixed for simplicity. The remaining free joints are shown on the right-hand side of Fig. 4. As a result, the remaining DOF was finally 51, which is larger than the DOF of the robot. The joint placement in the human model mainly differs from that in the robot in that it includes several redundant spherical joints in the human model to represent shoulder and spine movements.

Our method represents variation in human geometric parameters with several virtual mechanical joints that function as translational joints. We replaced parameters with virtual joints according to the diagram on the right side of Fig. 4. The feature points used in (10) are also illustrated in Fig. 4. They are generally located at the center of a joint or a point offset from the center of the joint, where the offsets have common values.

When evaluating assistive devices, the movement of the waist is often focused upon because some assistive devices are designed to support the waist in preventing back pain [5], [8]. The results of retargeting waist movements are presented in Sections IV-B1 to IV-B4. In order to check how the retargeting process performs with redundant joints, shoulder movement is also investigated in Section IV-B5. In summary, we recorded the following motions for our tests:

1) *Bending motion:* A subject bends forward from the waist with dumbbells in hand, and then returns to an upright position. Snapshots of the measured motion are shown in the top row of Fig. 5.
2) *Twisting motion:* A subject lifts up a light object placed in front of the right foot and sets it down on the left side by twisting at the waist (see Fig. 6).
3) *Arm motion:* A subject raises and moves the arms as if the subject were turning a handle located in front and above the head. Snapshots of the measured motion are shown in Section IV-B5.

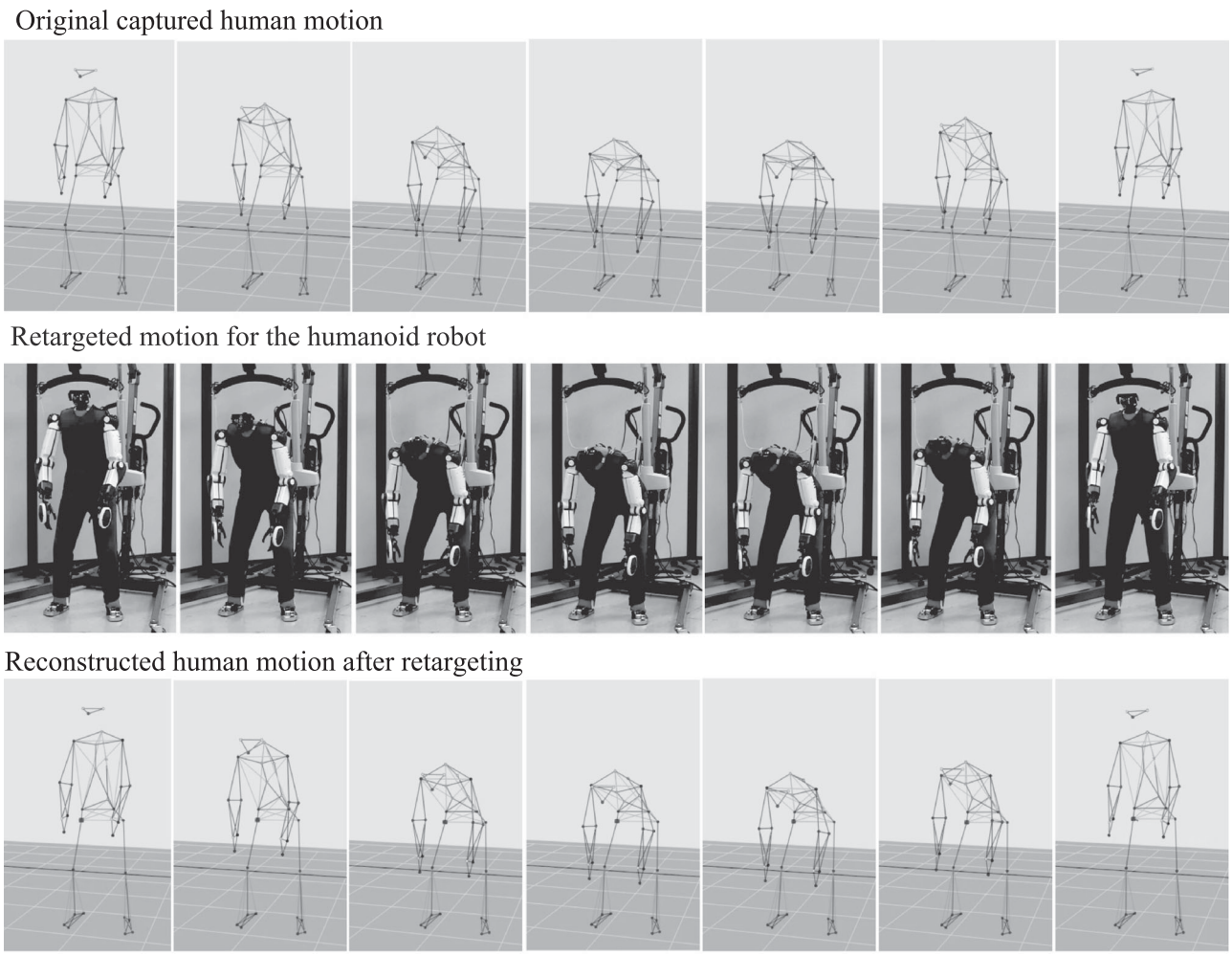

Fig. 5. Snapshots of bending forward motion. The figures in the top row show motion-capture data. The retargeted motion performed by the robot is pictured in the figures in the middle. The reconstructed markers from the retargeting result are shown in the bottom figures.

We recorded motions by several human subjects with motion-capture systems. When retargeting the motions according to (25), we used the following weighting factors: $\omega_\phi = 10$, $\omega_{g_k} = 100$, $\omega_{h_l} = 100$ for joint limits; $\omega_{h_l} = 100$ for ZMP constraints; $\omega_{h_l} = 500$ for COM constraints; $\omega_{h_l} = 500$ for foot contacts; and $\omega_{h_l} = 2$ for the constraints on the reaching task. The positions of the markers attached to the hands were used for references in the task constraints. In order to prevent the penalty function method from violating the inequality constraints of (25), we also added a safety margin to some of the inequality constraints; the margin for each joint angle limit was set at two degrees and that for the ZMP and COM was one centimeter.

Though the sampling period for the captured motions was originally 5 ms, we made the twisting and arm motions two times slower in the retargeting process; the data were resampled with a sampling period of 10 ms. We made this adjustment because the operating speed of the measured human joints exceeded the maximum speeds of several joints of the robot. Since our main focus is an analysis of the geometric features of the motion of each body segment, as shown in the cost function (25), we introduced this slow-down operation. However, this slow down can obscure the detailed dynamical features of quick motions in practice, so we will investigate an automatic method of time scaling within the constraints of speed limits in future work.

We solved (25) iteratively to generate motions in HRP-4. The computation time for each motion frame was kept within 30 ms for 1 step of whole-body motion by using an Intel(R) Core(TM) i7-4800MQ CPU (2.70 Gz). Before the robot actually performed the motions, we also checked that the joint angles, COM, ZMP did not violate the constraints in the simulation.

B. Experimental Results

1) Retargeting Results for Two Types of Waist Movements: The proposed method was tested first by retargeting the movements at the waist, the bending and twisting motions described above. The retargeted motions were successfully performed by HRP-4 while remaining upright, as the snapshots in the middle rows of Figs. 5 and 6 indicate. Our method can reconstruct the retargeted result and map it onto the original human marker positions, yielding a reconstructed motion that takes into account the modifications made to the original motion, according to (7). Snapshots of the reconstructed models are shown in the bottom rows of Figs. 5 and 6, which will be detailed in Sections IV-B3

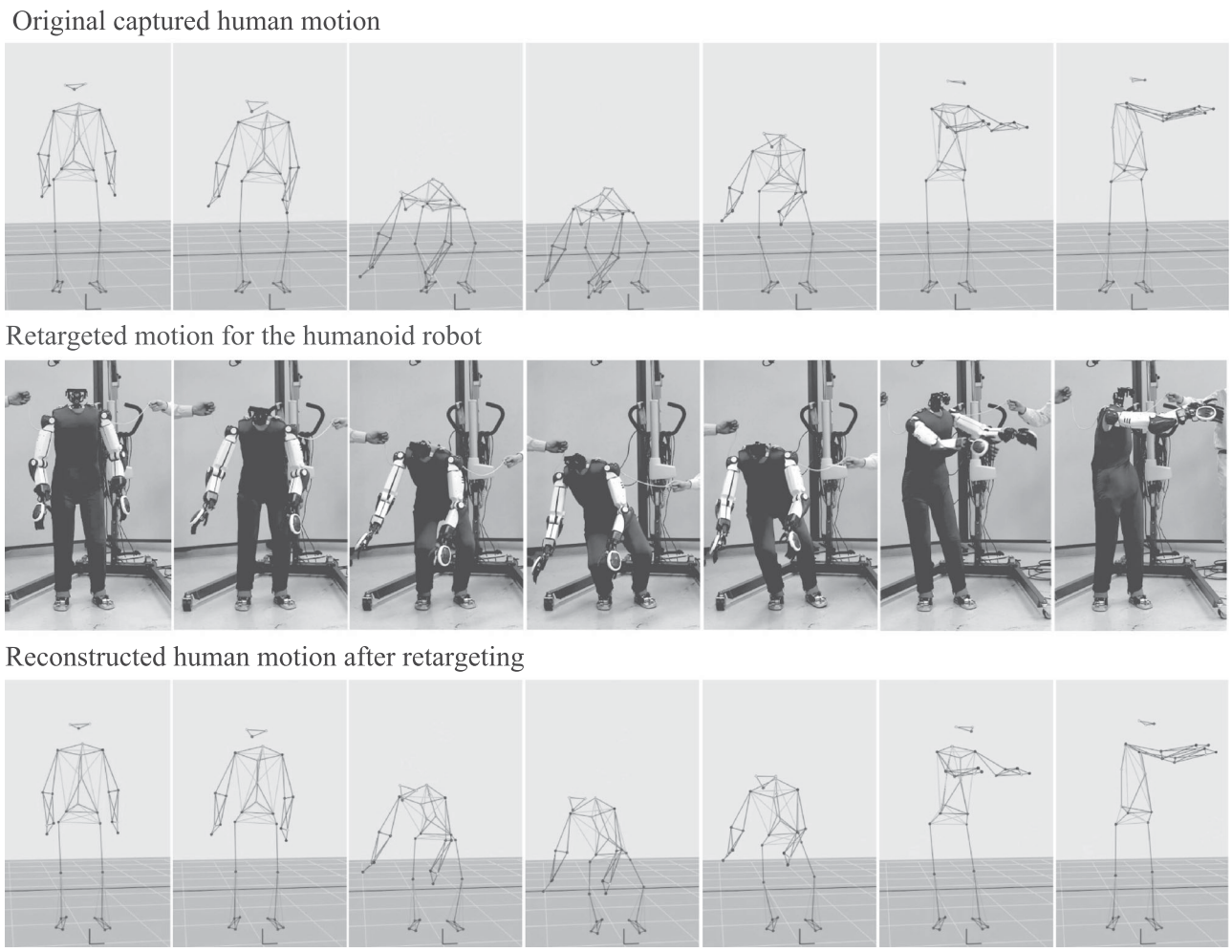

Fig. 6. Snapshots of twisting motion. Top: captured markers, Middle: retargeted motion, Bottom: reconstructed markers.

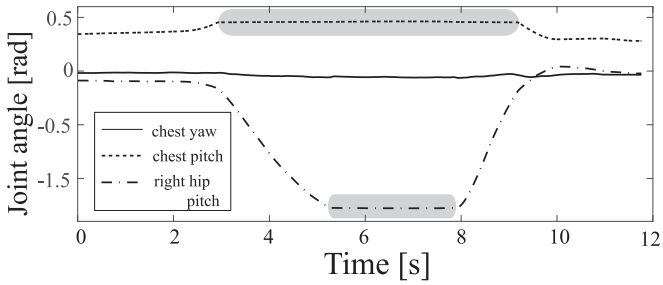

Fig. 7. Joint angles of the robot during the bending motion. The solid and dotted lines show the angle of the yaw and pitch axis of the chest joint, respectively. The dashed line is the pitch angle of the right hip joint. The joints reach their limits in the gray sections.

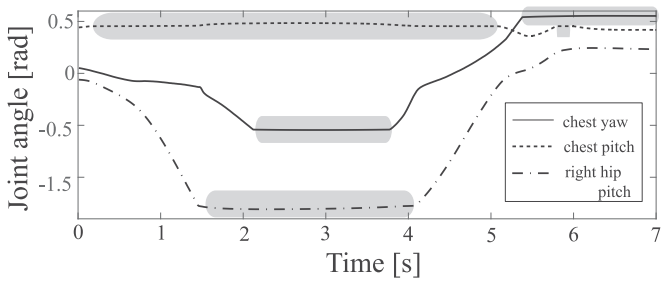

Fig. 8. Joint angles of the robot during the twisting motion.

and IV-B4. As can be seen from Fig. 5, the robot could mimic the posture of all body segments in a fashion quite similar to that of the measured human motion in all snapshots. The figures also show visible differences between the positions of the measured and reconstructed markers when bending deeply. These inaccuracies are due to limitations on the joint angles of HRP-4's chest- and hip-pitch joints. Fig. 7 shows the joint angle trajectories of the chest and hip joints during the bending motion. The chest-pitch joint stays at its maximum angle from 3 to 9 s; the hip-pitch joint maxes out from 5 to 8 s. Fig. 6 also shows that the twisting motion of the robot closely resembles the original human motion, except for the fourth and fifth snapshots. When bending deeply, the joints at the chest and hip of the robot reach their limits. Fig. 8 shows the joint angle trajectories of the chest and hip joints during the twisting motion. Limits on these joints cause the difference in trunk postures between the robot and the human. The snapshots indicate that the robot tried to perform the reaching task within the possible operational range of the joints; we can see in the retargeted and reconstructed motion

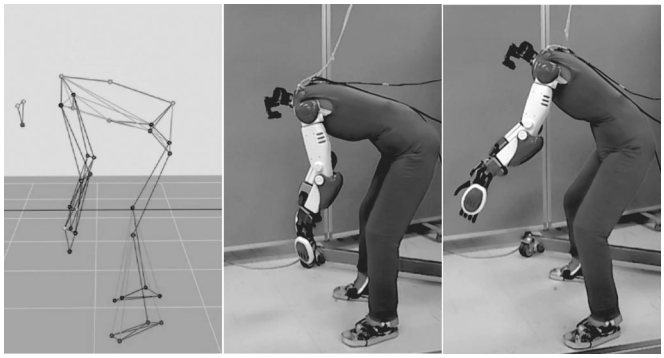

Fig. 9. Retargeting results from two optimization approaches: the left figure shows the measured human data, the middle one is the result given by the simultaneous optimization, and the right one shows the result obtained from the sequential optimization algorithm.

that the robot knees bended more deeply to compensate for the waist and chest limitations.

2) Comparison Between Simultaneous and Sequential Optimization: Next, we present an example of a motion for which our simultaneous optimization yields better performance than solving the optimization processes sequentially. The lifting motion was also retargeted by solving the sequential processes with the same physically consistent conditions. Function $\widehat{f}$ in (6) was implemented as the sum of the mean squared error between the two joint trajectories at each time instance.

One snapshot when the human subject bends deeply is shown on the left of Fig. 9. The corresponding robot postures are also shown in Fig. 9. The center figure shows the results of simultaneous optimization, and the right figure shows the result obtained from sequential optimization. Due to the joint-limit constraints on the hip and chest joints, the robot could not imitate the human motion exactly and needed to modify its own motion as shown in Fig. 7. The location and posture of the robot arms are significantly different in Fig. 9. As mentioned in Section II, when optimizing in sequence, the second optimization is performed only for the robot's physical constraints, which causes drift from the optimal solution of (4). This point is the advantage of the simultaneous optimization compared to the sequential approach.

3) Comparative Analysis in the Joint Space Using Reconstructed Human Motion: Our method can also provide a reconstructed human motion $\boldsymbol{Q}_h{}^*$ that corresponds to robot motion $\boldsymbol{Q}_r{}^*$. This step enables direct comparisons between the human joint coordinates during the original human motion and the coordinates the same human would traverse during the reconstructed motion. In addition, by utilizing inverse dynamics analysis for a human skeletal model [6], dynamical quantities such as joint torque can also be compared. This subsection focuses on the comparison of the waist joint movement of the human skeletal model during the lifting and twisting motions, since the waist joint plays an important role in such motions. The waist joint coordinate system is located at the L5 vertebra in the skeletal model, as shown in Fig. 10, where the initial posture of the bending motion is also shown. The waist joint is modeled by a spherical joint, as shown in Fig. 4. Note that HRP-4 has no waist joint but instead features rotational chest

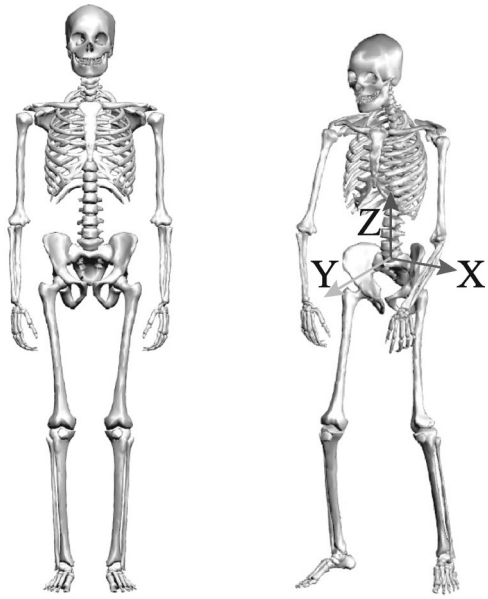

Fig. 10. Overview of human skeletal model. The left figure shows the initial posture of the model. The right one is the posture at the beginning of the lifting motion. The right figure also indicates the waist joint coordinates located at L5.

joints. The geometric offset between the human waist and robot chest joints is calibrated according to the morphing process.

The joint angles, velocities, and torques of the waist joint during the lifting and twisting motion are plotted in Figs. 11 and 12, respectively. The joint angles of the spherical joint are represented by *XYZ* Euler angles. The joint velocities represent the relative angular velocities of the joint coordinates with respect to their parent coordinates. In both figures, the top three graphs plot the components of the joint angles of the spherical joint, the middle three plot the joint velocities, and the bottom three graphs plot the joint torques. Solid lines indicate the values for the original human motion and the dotted ones indicate those of the reconstructed motion. Since the twisting motion was slowed down due to limitations of the robot hardware, the total times of the original human motion and the reconstructed motion differ, whereas the motion speeds were the same for the lifting motion. In order to compare the velocities and torques, each time axis is normalized to the total time period of the motion.

In Fig. 11, all components of the reconstructed values are close to those of the original ones, which indicates that the retargeted bending motion preserved the original pattern of the human trajectory. There is a slight difference in the joint angles when the normalized time is between 0.3 and 0.7. This divergence is due to the limits of robot chest joints, as discussed above. Slight differences in the joint velocities also occur due to a sudden change in the joint angles when reaching the limit. Fig. 12 shows that the reconstructed motion failed to preserve the geometric pattern along the *x*-axis. The error in the joint angle is large, especially when the normalized time is between 0.2 and 0.5. During this period, the robot's hip joint reached its limit and the human waist joint is assumed to compensate the generated error. Though the errors in the *y*- and *z*-axis angles are small, the same phenomenon appears. Since the reconstructed

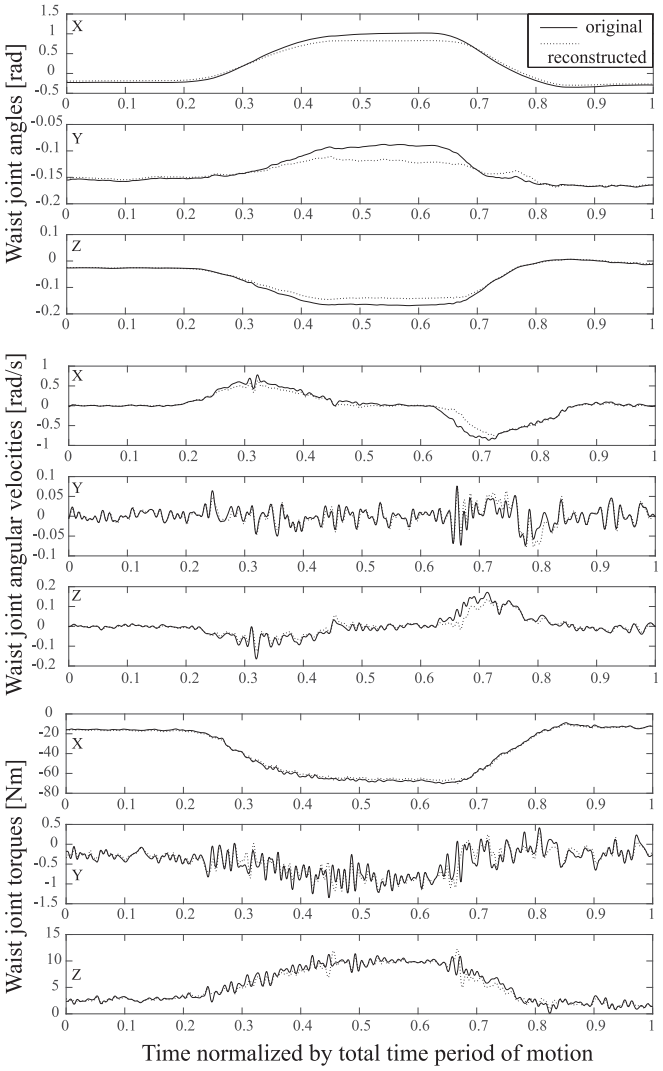

Fig. 11. Joint angles, velocities, and torques of the spherical waist joint during the lifting motion. The top three graphs show x, y, and z components of joint angles represented by XYZ Euler angles. The middle three graphs show the components of waist joint angular velocities and the bottom three plot waist joint torque. Solid lines indicate the values for the original human motion. The dotted lines represent the reconstructed human motion. The time axis is normalized to the total period of the motion. The total times of both the original and reconstructed motions are 11.8 s.

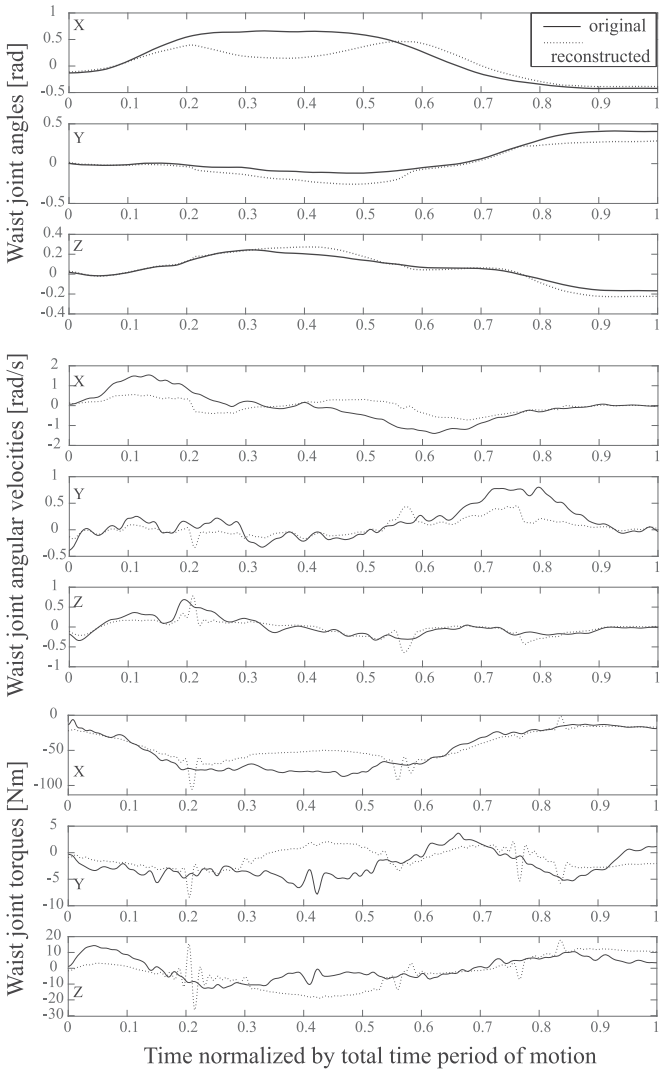

Fig. 12. Joint angles, velocities, and torques of the waist spherical joint during the twisting motion. Graph and line types are the same as those in Fig. 11. The total time of the original motion is 3.5 s, whereas that of the reconstructed one is 7.0 s.

twisting motion is two times slower than the original one, the joint velocities of the reconstructed motion are also two times smaller. In addition, a large acceleration occurs at the joint limitations of the robot, which generates impulses of the joint torque. The effect of the slowing down operation can be seen in the y- and z-axis joint torques. However, this effect is relatively small in the z-axis joint torque because the torque due to gravity in the twisting motion dominates the body's inertial torque. On the other hand, there is a large error in x-axis joint torque due to that in the joint angles when the normalized time is between 0.2 and 0.6. As can be seen from the above comparisons, our framework enables a quantitative comparative analysis of dynamical properties in addition to geometric features.

4) Comparative Analysis in Cartesian Space: We next check the robot's success in reaching Cartesian space during the two motions, by analyzing the positions of the markers attached to the tips of the robot's hand. Figs. 13 and 14 represent three types of marker positions: the markers measured from the original human subject (solid lines), the virtual markers attached to the robot (dotted lines), and the markers reconstructed onto the human model with the optimization results (dashed lines). The robot could perform the reaching task without significant modification from the original human motion except during the deepest bend. There is a small error in the z-direction (maximum 7.7 cm) due to the joint limits of the robot. Since the reconstructed motion is computed with the human geometric model, the error in the original measured data is smaller than that in the robot motion. Conversely, Fig. 14 shows large errors in the y- and z-directions between the original and retargeted motions (y: maximum 19.5 cm, z: maximum 36.7 cm); meanwhile, the error between the reconstructed and original motions is slightly smaller (y: maximum 18.0 cm, z: maximum 26.0 cm). The differences between the retargeted motion and the reconstructed

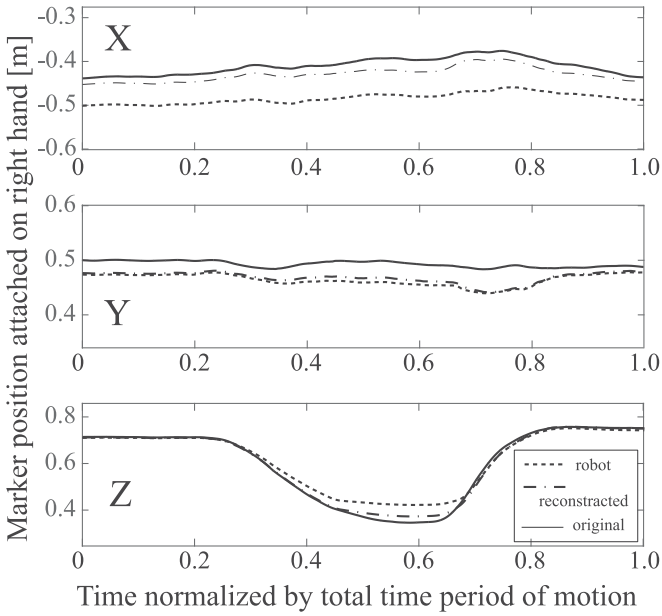

Fig. 13. Cartesian positions of the marker attached on the tip of the hand during the bending motion. The solid lines show the positions of the original human motion. The dotted lines mean the positions of the virtual markers attached on the robot model during the retargeted motion. The dashed lines indicate the reconstructed positions of the markers from the human model according to the result of the retargeting. The time axis is normalized by total time period of the motion. The total time of each motions is 11.8 [s].

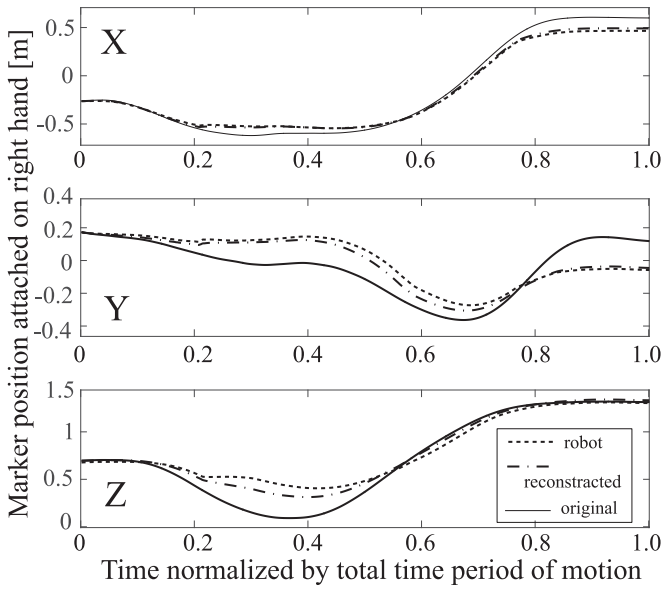

Fig. 14. Cartesian positions of the marker attached on the tip of the hand during the twisting motion; line types are the same as in Fig. 13. The total time of the original human motion is 3.5 [s], and the other two are 7.0 [s].

motion are due to the different geometric parameters of the human model and the robot. These results imply the following: for the twisting motion, the robot is limited in simultaneous movements involving the pitch and yaw axes of the waist and the *y*- and *z*-directions of the hand. These findings are useful for future improvements or novel robot hardware designs.

As mentioned in Section II, the reconstructed human motion originally reflects modifications according to the retargeting process. In other words, such reconstructed motions can be imitated by the robot without modification according to the constraints on the robot. Therefore, they can be regarded as candidate human motions that can be imitated by the robot without losing the original geometric features of the motion. If such reconstructed motions can be performed by an actual human subject, we can investigate the reconstructed motions using several techniques of human motion analysis, such as inverse dynamics analysis in Section IV-B3. For practical applications [5], we especially need to check whether the reconstructed twisting motion can be useful for the quantitative evaluation of assistive devices, which will be addressed in future work.

5) Comparison When Using Different Human Models: Since the mapping function can take an implicit form as shown in (1), which includes unknown geometric parameters, the total DOF of a human model can be different from that of the target robot. A redundant-jointed human model with 51 DOF in Fig. 4 was used in the experiments reported in the previous subsections. We now investigate the role played by the redundant joints in the human model in the proposed retargeting method.

Two different types of human models were examined in this validation. The first model is the same 51-DOF model that is shown on the right side of Fig. 4. The second model was prepared by locking the redundant DOF of the first model in order to realize the same 31 DOFs as the robot model. The main difference from the original model is that the sternoclavicular joints are fixed to the initial standing posture. An additional spherical joint on the thoracic spine in the 51-DOF model is also fixed at the initial posture. Some of the spherical joints in the original model, such as elbow and knee joints, are also changed to rotational ones in the second model.

The two human models were tested by retargeting an arm movement that resembles turning a handle located overhead. Snapshots of the measured human motion are shown at the top of Fig. 15. The retargeted results when using the 51- and the 31-DOF models are shown in the middle and bottom panels of Fig. 15, respectively. This arm movement is difficult to imitate due to the movement range of HRP-4. The retargeted motion when using the 51-DOF model appeared similar to the original motion. When retargeting with the 31-DOF model, however, the position and orientation of the right hand could often not be imitated, as shown in Fig. 15; in the original human motion, the palms are almost facing each other during the motion. The locations of the retargeted arms in the second case tend to be higher than those of the arms in the first case. The corresponding human marker trajectories were also reconstructed. The average position errors between the original and reconstructed markers are 2.2 cm in the first case and 3.2 cm in the second case. Therefore, retargeting with the 51-DOF redundant-jointed human model performed better.

Let us now check how each human model was mapped onto the robot model when retargeting the arm movements. The morphed human models are shown in Fig. 16; the left figure shows the morphed result of the 51-DOF model, whereas the right figure shows that of the 31-DOF model. In Fig. 16, the joint angles of the 31-DOF model are equal to those in the initial

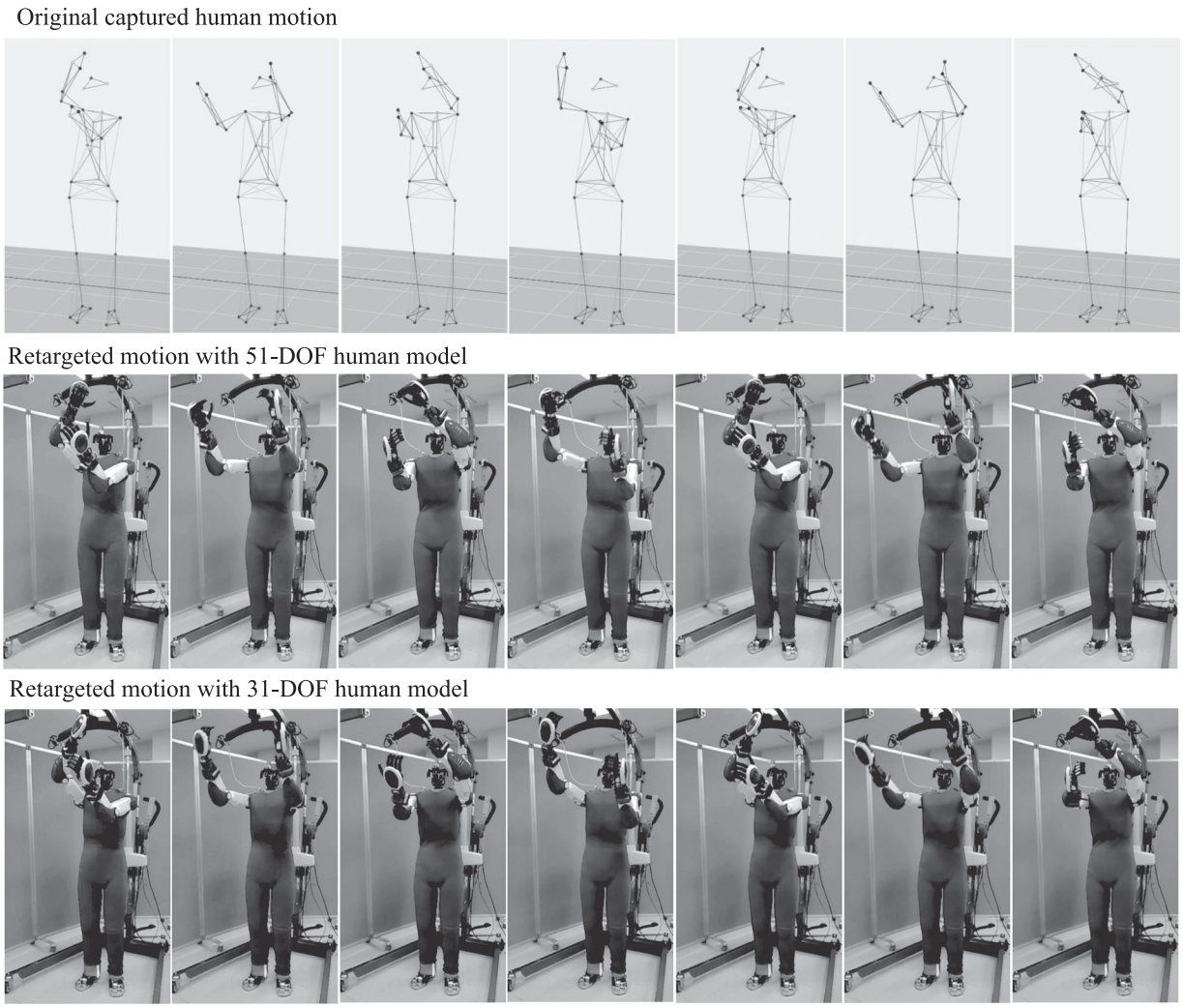

Fig. 15. Snapshots of arm motion. The figures in the top row show the captured motion. The retargeting results when using 51- and 31-DOF human models are given in the middle and bottom, respectively.

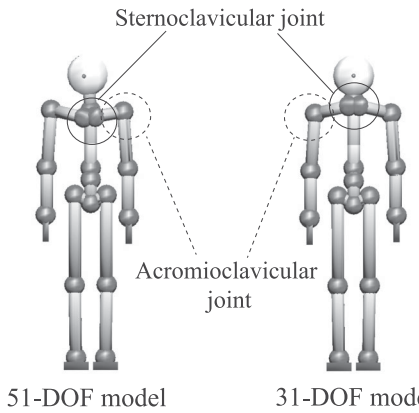

Fig. 16. Comparison of the morphed human models; the left figure shows the result when using the 51-DOF model, and the right one is obtained from the 31-DOF model.

standing posture. On the other hand, for the 51-DOF model, the redundant joints are constrained during the retargeting process, and finally, reach almost constant values, which are determined after the retargeting process. In the model of Fig. 16, the joint angles corresponding to the redundant-joint coordinates are set at the averaged values during the arm movement and the joint angles in the 31-DOF model remain the initial posture.

In the left figure of Fig. 16, the position of the acromioclavicular joints is higher than that of the sternoclavicular joints because the position of both arms stays higher than the shoulders during the handle-turning movement. The right side of Fig. 16 shows that the position of acromioclavicular joints is lower because their joint angles are fixed to the initial standing posture. The geometric parameters are modeled with virtual translational joints, as shown in Fig. 4; one virtual translational joint is located between the acromioclavicular and sternoclavicular joints. The coordinate of the sliding joint stands for the length between the two joints, and changing this value can scale the model along the axis connecting the two joints. In the configuration of the geometric parameters, the direction of the axis is fixed according to the initial posture during retargeting when using the 31-DOF model. On the other hand, in the case of the 51-DOF model, the direction of the axis connecting the two joints is determined according to the redundant joint angles obtained after motion

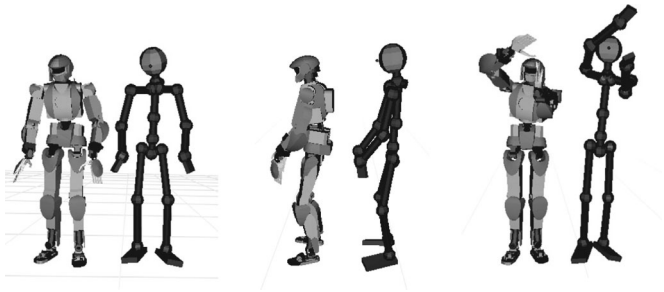

Fig. 17. Comparison of the body scale between the human subject model and the robot (left: twisting motion, middle: lifting motion, right: arm motion).

retargeting. This direction is optimal for minimizing the fitting error from the original human motion. If the best initial location of the shoulder joints can be determined in advance, the retargeting results with a 31-DOF model will be, of course, almost same as when using the 51-DOF model. The geometric parameter identification can automatically find the optimal parameters.

The above results can be summarized as follows. When modeling the human subject with redundant joints, the angles are constrained according to the morphing function. The constrained joint angles then serve as new morphing parameters that iteratively make the morphing function more exact. The optimal constrained joint angles can differ according to different human motions. The geometric parameter identification process can automatically find the best parameters.

Note that the geometric parameter identification process can accommodate differences in proportion among human subjects. A comparison of the body properties of the human subject model and the robot is visualized in Fig. 17, the left figure shows a pair of models performing the twisting motion, the middle illustrates the lifting motion, and the right shows the handle-turning movements. Different subjects provide motion-capture data for each motion. A 160-cm-tall subject performs the twisting motion, a 168-cm-tall subject performs the lifting motion, and a 174-cm tall subject performs the arm movement; the height of HRP-4 is 151 cm.

V. Conclusion

This paper has proposed a motion retargeting method for humanoid robots that preserves features of the original motion and serves up comparative evaluations of the results. Our method estimates geometric and morphing parameters simultaneously during motion retargeting in response to physically consistent conditions of the robot. While several related studies have solved the above problems sequentially, the proposed method solves them simultaneously as a single optimization problem. Simultaneous optimization offers better performance in matching the original human motion. The method also produces a human virtual motion that reflects the modifications required for the robot's range of motion and dynamical properties. This reconstructed virtual motion enables a quantitative analysis of the retargeting results through the direct comparison of the reconstructed motion and the original motion-capture data. The method can accommodate human models with more DOF than the robot model. Redundant joint angles such as shoulders are represented as pseudomorphing parameters, which enable precise morphing between the human and the robot. The simultaneous geometric identification algorithm provides their optimal values for geometric values as well as subject-specific parameters. Therefore, the method can accommodate the varying physical properties of individual human subjects.

We tested our method with the humanoid robot HRP-4, which could perform the retargeted motions without toppling over. To clarify the advantage of simultaneous optimization, we compared results of conventional sequential optimization with those of our simultaneous optimization algorithm; the simulations optimization showed better performance. We also reconstructed a human motion corresponding to the retargeted waist movement and compared angles, velocities, and torques of the waist joint and the Cartesian position of the hands. All these features were imitated accurately, except when bending deeply beyond the robot's range of motion. Such comparison clarifies that physical quantities are modified during the retargeting process. We also evaluated our framework by retargeting a complex arm movement. We used two human models, one with the same DOF as that of the robot and the other with several redundant joints. The redundant jointed human model performed better because of the redundant shoulder joints. This test also showed that the geometric parameter identification algorithm can handle various sizes of human subjects.

The reconstructed virtual motion can help us to identify candidate human motions that the robot can imitate well within its operational range. Though the paper mainly focuses on retargeting geometric features, the retargeting of dynamical features such as forces and ZMP is a topic for future research. We expect to generalize the proposed optimization framework by incorporating identification techniques for inertial parameters [31] in future work.

For applications such as evaluating assistive devices [5], robot must imitate human motion as closely as possible. Such evaluations for industrial standards require quantitative evaluation criteria for the accuracy of a robot imitation, which the method above provides. We have also begun to test the proposed retargeting method on an actual evaluation of assistive devices with a humanoid robot [32], [33]. We also propose to investigate the usefulness of having human subjects perform motions reconstructed from the retargeted process in the future.

Acknowledgment

The authors would like to express sincere gratitude to Dr. M. Morisawa of AIST for his support and advice for the humanoid experiments.

References

[1] J. Lim *et al.*, "Robot system of DRC-HUBO+ and control strategy of team KAIST in DARPA robotics challenge finals," *J. Field Robot.*, vol. 34, no. 4, pp. 802–829, 2016.

[2] S. Nakaoka *et al.*, "Learning from observation paradigm: Leg task models for enabling a biped humanoid robot to imitate human dances," *Int. J. Robot. Res.*, vol. 26, no. 8, pp. 829–844, 2007.

[3] K. Miura *et al.*, "Robot motion remix based on motion capture data towards human-like locomotion of humanoid robots," in *Proc. IEEE-RAS Int. Conf. Humanoid Robots*, 2009, pp. 596–603.
[4] A. Omer, H. Kondo, H. Ok Lim, and A. Takanishi, "Development of walking support system based on dynamic simulation," in *Proc. IEEE Int. Conf. Robot. Biomimetics*, 2009, pp. 137–142.
[5] K. Miura *et al.*, "Humanoid robot as an evaluator of assistive devices," in *Proc. IEEE Int. Conf. Robot. Autom.*, 2013, pp. 671–677.
[6] Y. Nakamura, K. Yamane, K. Fujita, and I. Suzuki, "Somatosensory computation for man-machine interface from motion-capture data and musculoskeletal human model," *IEEE Trans. Robot.*, vol. 21, no. 1, pp. 58–66, Feb. 2005.
[7] S. L. Delp *et al.*, "Opensim: Open-source software to create and analyze dynamic simulations of movement," *IEEE Trans. Biomed. Eng.*, vol. 54, no. 11, pp. 1940–1950, Nov. 2007.
[8] Y. Imamura, T. Tanaka, Y. Suzuki, K. Takizawa, and M. Yamanaka, "Motion-based-design of elastic material for passive assistive device using musculoskeletal model," *J. Robot. Mechatronics*, vol. 23, no. 6, pp. 58–66, 2011.
[9] Y. Yoshiyasu, K. Ayusawa, E. Yoshida, Y. Matsumoto, and Y. Endo, "Forward dynamics simulation of human figures on assistive devices using geometric skin deformation model," in *Proc. IEEE Annu. Int. Conf. Eng. Med. Biol. Soc.*, 2015, pp. 2442–2445.
[10] K. Kaneko, F. Kanehiro, M. Morisawa, K. Miura, S. Nakaoka, and S. Kajita, "Cybernetic human HRP-4C," in *Proc. IEEE-RAS Int. Conf. Humanoid Robots*, 2009, pp. 7–14.
[11] K. Kaneko *et al.*, "Humanoid robot HRP-4—Humanoid robotics platform with lightweight and slim body," in *Proc. IEEE/RSJ Int. Conf. Intell. Robots Syst.*, 2011, pp. 4400–4407.
[12] M. Gleicher, "Retargetting motion to new characters," in *Proc. 25th Annu. Conf. Comput. Graph. Interactive Techn.*, 1998, pp. 33–42.
[13] N. Pollard, J. Hodgins, M. Riley, and C. Atkeson, "Adapting human motion for the control of a humanoid robot," in *Proc. IEEE Int. Conf. Robot. Autom.*, 2002, pp. 1390–1397.
[14] C. Ott, D. Lee, and Y. Nakamura, "Motion capture based human motion recognition and imitation by direct marker control," in *Proc. IEEE-RAS Int. Conf. Humanoid Robots*, 2008, pp. 399–405.
[15] B. Dariush *et al.*, "Online transfer of human motion to humanoids," *Int. J. Humanoid Robot.*, vol. 6, no. 2, pp. 265–289, 2009.
[16] K. Yamane, S. Anderson, and J. Hodgins, "Controlling humanoid robots with human motion data: Experimental validation," in *Proc. IEEE-RAS Int. Conf. Humanoid Robots*, 2010, pp. 504–510.
[17] O. Ramos, L. Saab, S. Hak, and N. Mansard, "Dynamic motion capture and edition using a stack of tasks," in *Proc. IEEE-RAS Int. Conf. Humanoid Robots*, 2011, pp. 224–230.
[18] S. Nakaoka and T. Komura, "Interaction mesh based motion adaptation for biped humanoid robots," in *Proc. IEEE-RAS Int. Conf. Humanoid Robots*, 2012, pp. 625–631.
[19] T. Moulard, E. Yoshida, and S. Nakaoka, "Optimization-based motion retargeting integrating spatial and dynamic constraints for humanoid," in *Proc. Int. Symp. Robot.*, 2013, pp. 1–6.
[20] G.-B. Hammam, P.-M. Wensing, B. Dariush, and E.-D. Orin, "Kino-dynamically consistent motion retargeting for humanoids," *Int. J. Humanoid Robot.*, vol. 12, no. 4, 2015, Art. no. 1550017.
[21] M. Vukobratovic, A. Frank, and D. Juricic, "On the stability of biped locomotion," *IEEE Trans. Biomed. Eng.*, vol. BME-17, no. 1, pp. 25–36, Jan. 1970.
[22] K. Ayusawa, M. Morisawa, and E. Yoshida, "Motion retargeting for humanoid robots based on identification to preserve and reproduce human motion features," in *Proc. IEEE/RSJ Int. Conf. Intell. Robots Syst.*, 2015, pp. 2774–2779.
[23] S. Gamage and J. Lasenby, "New least squares solutions for estimating the average centre of rotation and the axis of rotation," *J. Biomech.*, vol. 35, no. 1, pp. 87–93, 2002.
[24] A. Kirk, J. O'Brien, and D. Forsyth, "Skeletal parameter estimation from optical motion capture data," in *Proc. IEEE Comput. Soc. Conf. Comput. Vis. Pattern Recognit.*, 2005, vol. 2, pp. 782–788.
[25] K. Ayusawa, Y. Ikegami, and Y. Nakamura, "Simultaneous global inverse kinematics and geometric parameter identification of human skeletal model from motion capture data," *Mech. Mach. Theory*, vol. 74, pp. 274–284, 2014.
[26] F. Basoeki, F. DallaLibera, and H. Ishiguro, "On the human perception of dissimilarities between postures of humanoids," *Adv. Robot.*, vol. 30, no. 21, pp. 1395–1405, 2016.
[27] T. Sugihara, Y. Nakamura, and H. Inoue, "Real-time humanoid motion generation through ZMP manipulation based on inverted pendulum control," in *Proc. IEEE Int. Conf. Robot. Autom.*, 2002, pp. 1404–1409.
[28] S. Kajita, F. Kanehiro, P. Kaneko, K. Yokoi, and H. Hirukawa, "The 3D linear inverted pendulum mode: A simple modeling for a biped walking pattern generation," in *Proc. IEEE/RSJ Int. Conf. Intell. Robots Syst.*, 2001, pp. 239–246.
[29] R. Fletcher, *Practical Methods of Optimization*, 2nd Ed. New York, NY, USA: Wiley, 1987.
[30] K. Ayusawa and Y. Nakamura, "Fast inverse kinematics algorithm for large DOF system with decomposed gradient computation based on recursive formulation of equilibrium," in *Proc. IEEE/RSJ Int. Conf. Intell. Robots Syst.*, 2012, pp. 3447–3452.
[31] K. Ayusawa, G. Venture, and Y. Nakamura, "Identifiability and identification of inertial parameters using the underactuated base-link dynamics for legged multibody systems," *Int. J. Robot. Res.*, vol. 33, no. 3, pp. 446–468, 2014.
[32] K. Ayusawa, E. Yoshida, Y. Imamura, and T. Tanaka, "New evaluation framework for human-assistive devices based on humanoid robotics," *Adv. Robot.*, vol. 30, no. 8, pp. 519–534, 2016.
[33] T. Ito, K. Ayusawa, E. Yoshida, and H. Kobayashi, "Stationary torque replacement for evaluation of active assistive devices using humanoid," in *Proc. IEEE-RAS Int. Conf. Humanoid Robots*, 2016, pp. 739–744.

Ko Ayusawa (M'17) received the B.S. degree in mechanical engineering, and the M.S. and Ph.D. degrees in mechano-informatics, from University of Tokyo, Tokyo, Japan, in 2006, 2008, and 2011, respectively.

He was with the Department of MechanoInformatics, University of Tokyo, as a Postdoctoral Researcher from 2011 to 2012, and as a Project Assistant Processor in 2013. He is currently a Researcher with the Intelligent Systems Research Institute, National Institute of Advanced Industrial Science and Technology (AIST), Tsukuba, Japan, and a Researcher of CNRS-AIST JRL (Joint Robotics Laboratory), UMI3218/RL. His research interests include the identification of human/humanoid dynamics, motion control for humanoid robots, and kinematics and dynamics simulation for human musculoskeletal models.

Eiichi Yoshida (SM'12) received the M.E. and Ph.D. degrees on precision machinery engineering from Graduate School of Engineering, University of Tokyo, Tokyo, Japan, in 1993 and 1996, respectively.

In 1996, he joined former Mechanical Engineering Laboratory, later reorganized as National Institute of Advanced Industrial Science and Technology (AIST), Tsukuba, Japan. He served as Co-Director of AIST/IS-CNRS/ST2I Joint French-Japanese Robotics Laboratory (JRL) at LAAS-CNRS, Toulouse, France, from 2004 to 2008. Since 2009, he has been Co-Director of CNRS-AIST JRL, UMI3218/RL, and since 2015 he has been Deputy-Director of Intelligent Systems Research Institute, AIST, Tsukuba, Japan. His research interests include robot task and motion planning, human modeling, and humanoid robots.